

## First-principles study of mechanical and magnetic properties of transition metal (M) nitrides in the cubic $M_4N$ structure



V. Adhikari<sup>a</sup>, Z.T.Y. Liu<sup>a</sup>, N.J. Szymanski<sup>a</sup>, I. Khatri<sup>a</sup>, D. Gall<sup>b</sup>, P. Sarin<sup>c</sup>, S.V. Khare<sup>a,\*</sup>

<sup>a</sup> Department of Physics and Astronomy, The University of Toledo, 2801 West Bancroft Street, Toledo, OH 43606, USA

<sup>b</sup> Department of Materials Science and Engineering, Rensselaer Polytechnic Institute, 110 8th Street, Troy, NY 12180, USA

<sup>c</sup> School of Materials Science and Engineering, Oklahoma State University, Tulsa, OK 74106, USA

### ABSTRACT

We report results from systematic calculations performed by density functional theory on mechanical properties of twenty-eight 3d, 4d and 5d transition metal (M) nitrides (TMNs) in metal-rich cubic  $M_4N$  structure as novel candidates for hard coatings materials. We have computed lattice constants, elastic constants, derived moduli and ratios which characterize mechanical properties, and other properties like magnetic moments, formation energies, Debye temperature and Bader charge transfer. Our calculations indicate that all  $M_4N$ -type metal nitrides except  $V_4N$ ,  $Nb_4N$ , and  $Pt_4N$  are mechanically stable. All Group 7 TMNs in the  $M_4N$  structure are found to have high Vickers hardness values with the highest being 24.3 GPa for  $Re_4N$ . Our computed lattice constants and magnetic dipole moments for  $Mn_4N$  and  $Fe_4N$ , the two compounds for which experimental measurements exist, are consistent with their measured values. Spin-polarized computations reduce the hardness of some magnetic compounds like  $Mn_4N$  and  $Fe_4N$ . The total density of states calculation reveals that all 28  $M_4N$  phases are metallic. The hybridization of metal d and nitrogen 2p orbitals is found to be the key factor in determining mechanical stability and hardness in these compounds. In contrast, ionicity, as computed by Bader charge transfer, does not correlate with hardness. Our comprehensive database for binary transition metal nitrides in  $M_4N$  structure offers wide possibilities for experimental synthesis of such materials with desirable physical properties for the hard-coatings application.

### 1. Introduction

In the last couple of decades, transition metal nitrides (TMNs) have been identified as promising materials for hard coatings application due to their excellent mechanical, wear and oxidation resistant properties [1–7]. Some experimentally synthesized novel TMNs like platinum nitride [8,9], osmium nitride ( $OsN_2$ ) [10,11] and iridium nitride [8,11,12] have been found to possess superior hardness. Other experimentally synthesized and studied promising candidates of TMNs include the nitrides of Sc [13–17], Y [18], Ti [19–22], Zr [6,23,24], Hf [6,23,25], V [26,27], Nb [6], Ta [28–31], Cr [30,32–35], Mo [30,33,36–38], W [29,33,39], Re [40,41], Fe [42], Pd [12,43], Cu [1], Au [44–47] and Zn [48]. Apart from experimental studies, theoretical computations can be useful in predicting mechanically stable superhard TMNs compounds and their properties. Such systematic theoretical studies not only provide information from which trends and correlations between the properties can be deduced but also save a considerable amount of effort, time and expense in experimental discoveries of new materials by narrowing the search for mechanically

and thermodynamically stable phases and their atomic structures. First principles calculations have been focused on the search of hard phases among binary TMNs in the B1 (rocksalt), and B2 (cesium chloride) structures with a stoichiometry of 1:1 (metal M: nitrogen N) and in the fluorite and pyrite structures of stoichiometry 2:1 [49–54]. Zhou et al. studied an anti- $ReO_3$  structure with a formula unit  $M_3N$  [55]. It is derived from the B1 structure by removing one metal atom on the corner and three nitrogen atoms on the edge centers. It is well recognized from such work that there is a large range of the M: N ratio where TMN phases remain stable. The quest for new binary TMNs with superior mechanical properties used in the hard coatings requires the expansion of this database for other compositions. This work is an attempt in this direction to speed the experimental discoveries of such phases.

The only two experimentally synthesized phases  $Mn_4N$  and  $Fe_4N$  of the  $M_4N$  type have motivated our study of this structure. The magnetic structure of  $Mn_4N$  was first determined in 1960 by Takei et al. [56] using neutron diffraction experiments and later Mekata et al. [57] obtained information on the electronic structure and magnetic properties of  $Mn_4N$ . Also, Frazer et al. [58] first explored the magnetic structure of

\* Corresponding author.

E-mail address: [sanjay.khare@utoledo.edu](mailto:sanjay.khare@utoledo.edu) (S.V. Khare).

Fe<sub>4</sub>N in 1958. These compounds along with their derivatives [57,59–61] are being explored for magnetic information storage applications. However, the superior mechanical properties of some TMNs [42,60–63] have led us to investigate methodically the M<sub>4</sub>N structure of 28 M<sub>4</sub>N type nitrides to search for hard coating materials in this structure type. We have generated an entire database of properties for these materials from first principles computations. Our database includes mechanical properties such as lattice constant, elastic constants, bulk modulus, shear modulus, Young's modulus, Poisson's ratio, Pugh's ratio, Vickers hardness along with the magnetic moments, Debye temperature, formation energy and electronic properties. Except for the two compounds Mn<sub>4</sub>N and Fe<sub>4</sub>N, no experimental or theoretical reports have been found in the literature for other remaining M<sub>4</sub>N compounds. The rich computational database of results for M<sub>4</sub>N compounds should prompt more experimental research in this structure for hard coatings applications.

## 2. Computational methods

The calculations were performed with a density-functional theory based Vienna *Ab initio* Simulation Package (VASP) [64–67] on 28 M<sub>4</sub>N-type transition metal nitrides. The following potentials with the projector augmented wave (PAW) [68,69] method under Perdew-Burke-Ernzerhof (PBE) generalized gradient approximation (GGA) [70,71] were applied for transition metals from VASP potential database [72]: Sc<sub>sv</sub>, Ti<sub>sv</sub>, V<sub>sv</sub>, Cr<sub>pv</sub>, Mn<sub>pv</sub>, Fe, Co, Ni, Cu, Zn for the 3 d row, Y<sub>sv</sub>, Zr<sub>sv</sub>, Nb<sub>sv</sub>, Mo<sub>pv</sub>, Tc<sub>pv</sub>, Ru<sub>pv</sub>, Rh<sub>pv</sub>, Pd, Ag, Cd for the 4 d row, and Hf<sub>pv</sub>, Ta<sub>pv</sub>, W<sub>pv</sub>, Re, Os, Ir, Pt, Au for the 5 d row, where the “\_sv” notation stands for the potentials with semi-core *s* and *p* electronic orbitals, and the “\_pv” notation for those with semi-core *p* electronic orbitals. A kinetic energy cut-off of 400 eV was selected for the plane wave basis set expansion of valence electron wave functions for all 28 compounds and a Monkhorst-Pack *k*-points grid [73–76] of density 11 × 11 × 11 was used. A Gaussian smearing of smearing width 0.1 eV was used for the electronic minimization with the convergence criterion set to 10<sup>−5</sup> eV/atom. Ionic relaxation was performed using a conjugate-gradient algorithm with a force criterion of 0.01 eV/Å as described in earlier works [53–55,77,78].

In order to perform stepwise large-scale simulations for 28 compounds, two robust Python workflow packages; pyvasp-workflow [79] and pydass\_vasp [80] were used. These are partially based on an open source project pymatgen [81], which is an open-source Python library for materials analysis acting as an interface between Python objects and input and output files of VASP.

For precise computation of equilibrium volume, *V*<sub>0</sub>, a set of runs varying the volume close to and bracketing a guessed equilibrium volume, *V*<sub>0g</sub>, under zero pressure was performed and the volume-energy data was fitted to the energy-volume form of the 3rd order Birch-Murnaghan [82,83] equation of state. We iteratively generated a good volume range to bracket *V*<sub>0</sub>. Thus, the precise equilibrium volume *V*<sub>0</sub> was determined for each of the 28 compounds in the same structure, with a well-fitted energy-volume curve and accurate final fitted parameters. Finally, knowing *V*<sub>0</sub>, the total energy of the cell in equilibrium was calculated.

To compute the three independent elastic constants, *C*<sub>11</sub>, *C*<sub>12</sub> and *C*<sub>44</sub> for the cubic crystal system, the 2nd order polynomial fitting of the energy-strain method [53–55,78] was employed. Three sets of strains were applied to the unit cell of each optimized compound allowing full relaxation of the ions to their equilibrium position. The strain tensor has the general form as:

$$\varepsilon_{ij} = \begin{pmatrix} e_1 & \frac{e_6}{2} & \frac{e_5}{2} \\ \frac{e_6}{2} & e_2 & \frac{e_4}{2} \\ \frac{e_5}{2} & \frac{e_4}{2} & e_3 \end{pmatrix} \quad (1)$$

**Table 1**

The three sets of elastic strains (*e*<sub>*i*</sub>) as denoted in Eq. (1), and the corresponding total energy change per unit volume ( $\Delta E/V_0$ ) expressed in terms of the three independent elastic constants (*C*<sub>11</sub>, *C*<sub>12</sub>, and *C*<sub>44</sub>) for the cubic system. The strain value | $\delta$ | is varied below 6%.

Strain	Non-zero Strain Elements	$\Delta E/V_0$
1	$e_1 = e_2 = e_3 = \delta$	$[3(C_{11} + 2C_{12}) \delta^2]/2$
2	$e_1 = \delta, e_2 = -\delta, e_3 = \delta^2/(1 - \delta^2)$	$(C_{11} - C_{12}) \delta^2$
3	$e_6 = \delta, e_3 = \delta^2/(4 - \delta^2)$	$(C_{44} \delta^2)/2$

The strain sets are described in Table 1. One is equivalent to the deformation under a hydrostatic pressure, i.e. volumetric change from the last step. The other two follow the forms of Eq. (11) and Eq. (13) of Mehl et al. [84]. For each set, we applied strain to the unit cell of 4 different values chosen to be below a maximum of 6%. The total energies of the strained cells were fitted to a parabolic curve as a function of strain. The second order coefficients of the fit so obtained yield values of *C*<sub>11</sub> + 2*C*<sub>12</sub>, *C*<sub>11</sub> − *C*<sub>12</sub> and *C*<sub>44</sub>, from which the three elastic constants were calculated as detailed in Patil et al. [49].

Other derived mechanical properties of the mechanically stable compounds were calculated using these elastic constants. Bulk modulus (*B*) is given by  $B = (C_{11} + 2C_{12})/3$ . The polycrystalline shear modulus in Voigt approximation (*G*<sub>V</sub>), Reuss approximation (*G*<sub>R</sub>) and Hill's arithmetic mean (*G*) is given by,

$$G_V = [(C_{11} - C_{12}) + 3C_{44}]/5, \quad (2)$$

$$G_R = [5(C_{11} - C_{12}) C_{44}]/(4C_{44} + 3C_{11} - 3C_{12}), \quad (3)$$

$$G = (G_V + G_R)/2. \quad (4)$$

Using these quantities, we also calculated Pugh's ratio (*k*) as  $k = G/B$ , Poisson's ratio ( $\nu$ ) as  $\nu = (3 - 2k)/[2(3 + k)]$ , Young's modulus (*E*) as  $E = 9G/(3 + k)$ . The Vickers hardness (*H*<sub>V</sub>) was calculated using the modified form of equation by Tian et al. [85], which always yields a positive value as:

$$H_V = 0.92k^{1.137}G^{0.708} \quad (5)$$

Also, the Debye temperature ( $\theta_D$ ) can be related to *G* and *B* through the speed of sound as given by the following equations:

$$\theta_D = \frac{h}{k_B} \left[ \frac{3n}{4\pi} \left( \frac{N_A \rho}{M} \right) \right]^{1/3} v_m \quad (6)$$

where,

$$v_m = \left[ \frac{1}{3} \left( \frac{2}{v_t^3} + \frac{1}{v_l^3} \right) \right]^{-1/3} \quad (7)$$

$$v_t = \left( \frac{G}{\rho} \right)^{1/2} \quad \text{and} \quad v_l = \left( \frac{3B + 4G}{3\rho} \right)^{1/2} \quad (8)$$

Here, *h* is Planck's constant, *k*<sub>B</sub> is Boltzmann's constant, *n* is the number of atoms in the primitive cell having molecular weight *M*, *N*<sub>A</sub> is Avogadro's number  $\rho$  is mass density, and *v*<sub>t</sub>, *v*<sub>l</sub> and *v*<sub>m</sub> respectively are transverse, longitudinal and mean sound speed [53].

As the Debye temperature and hardness both depend on the nature of atomic bonding in the crystal, a relation between these two quantities is given by the following equation of Deus and Schneider [86]:

$$\theta_D = a \times H_V^{1/2} \rho^{-1/6} M^{-1/3} + b \quad (9)$$

where *a* and *b* are linear fitting coefficients.

Keeping in mind that the consideration of magnetism due to electron's spin magnetic moments can greatly influence the structural stability of a compound [87] and the elastic and mechanical properties simply depend on the structure, we included magnetism for all the compounds, assuming ferromagnetism during the volume determination step. If the structure at the equilibrium volume showed a non-zero

magnetic moment, magnetism was again considered during the next steps. Nitrides of 3d transition metal Sc, Mn, Fe, Co, Ni are expected to exhibit variation in their mechanical properties with consideration of magnetic phases. We thus report a comparison between values for elastic properties calculated with and without the consideration of magnetism for these phases.

For all 28 compounds, we used Bader charge analysis [88–91] and Bader's division scheme [92,93] to observe the trend in the charge transfer from metal atoms to the nitrogen atom. An FFT grid of  $200 \times 200 \times 200$  was used to extract valid results of charge transfer. The total density of states (TDOS) for all 28  $M_4N$ -type metal nitrides and local density of states (LDOS) for the three hardest compounds  $Mn_4N$ ,  $Tc_4N$  and  $Re_4N$  were calculated with GGA using tetrahedron method with Bloch corrections [94]. The phonon densities of states were also computed for two compounds,  $Mn_4N$  and  $V_4N$ , by creating  $2 \times 2 \times 2$  supercells and calculating the corresponding Hessian matrices using density functional perturbation theory (DFPT) [64–67] and the PHONOPY code [95].

### 3. Results and discussion

#### 3.1. Mechanical properties

The chemical structure of cubic  $M_4N$  compounds (space group  $Pm\bar{3}m$ ) can be derived from the B1 (rocksalt) structure of MN where, the metal sub-lattice is kept intact, and the three nitrogen atoms on the edge centers are removed from the B1 structure. Thus, the primitive cell of  $M_4N$ -type transition metal nitride consists of 4 M atoms and one N atom where, M atoms occupy the points of a face centered cubic lattice with N atom at the body-centered position of the unit cell. This  $M_4N$ -type structure is shown in the ball-and-stick representation in Fig. 1, where the sticks are bonds of the N atom to the nearest M atoms. The N atom forms an octahedral coordinated by 6 M atoms, which is shown as the shaded polyhedron. Experimental and theoretical values exist for only two magnetic compounds  $Mn_4N$  and  $Fe_4N$ . We present, in Table 2, a comparison between the calculated and experimental values of lattice constant ( $a$ ), elastic constants ( $C_{11}$ ,  $C_{12}$ ,  $C_{44}$ ) and total magnetic moment (Mag.) in Bohr magnetons ( $\mu_B$ ) per formula unit for these two

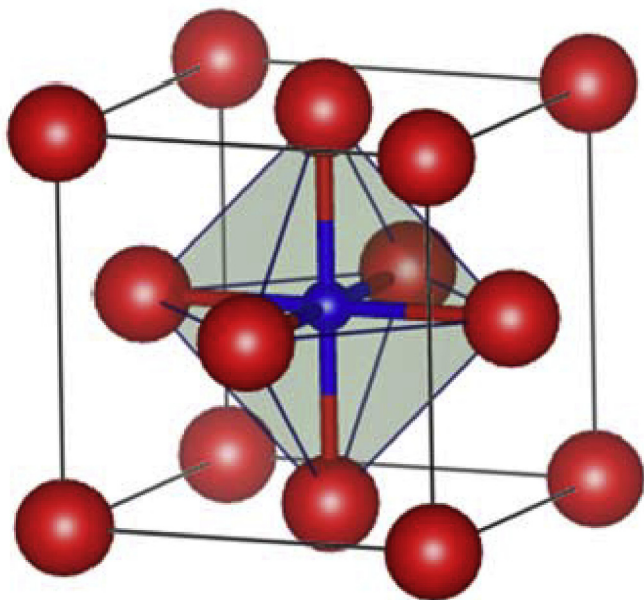


Fig. 1. Structure of  $M_4N$  compound, where the large red balls represent the transition metal (M) atoms and smaller blue ball represents nitrogen (N) atom. (For interpretation of the references to colour in this figure legend, the reader is referred to the Web version of this article.)

Table 2

A Comparison of calculated values of lattice constant ( $a$ ), total magnetic moment (Mag.) in Bohr magnetons ( $\mu_B$ ) per formula unit and elastic constants ( $C_{11}$ ,  $C_{12}$ ,  $C_{44}$ ) of  $Fe_4N$  and  $Mn_4N$  with values from experiments and first principles.

	$a$ (Å)	Mag. ( $\mu_B$ )	$C_{11}$ (GPa)	$C_{12}$ (GPa)	$C_{44}$ (GPa)
<b><math>Mn_4N</math></b>					
This work	3.744	1.19	452.7	103.3	120.4
Exp. <sup>a</sup>	3.87	1.2			
Exp. <sup>b</sup>	3.865	1.1			
<b><math>Fe_4N</math></b>					
This work	3.795	9.84	305.9	140.7	44.6
Exp. <sup>c</sup>	3.797	9.01			
Exp. <sup>d</sup>	3.790				
Exp. <sup>e</sup>		9.45			
USPP-PBE <sup>f</sup>	3.780	10.01	322.8	132	48.3
PAW-GGA <sup>g</sup>	3.792		313	137	46

<sup>a</sup> Ref. [57].

<sup>b</sup> Ref. [56].

<sup>c</sup> Ref. [58].

<sup>d</sup> Ref. [96].

<sup>e</sup> Ref. [97].

<sup>f</sup> Ref. [59].

<sup>g</sup> Ref. [62].

compounds. Our calculated values of lattice constant and magnetic moment for  $Mn_4N$  and  $Fe_4N$  agree well with their experimental [56–58,96,97] and calculated [59,62] values in the literature. For the remaining  $M_4N$  compounds, previous experimental or theoretical data are not available.

Table 3 shows the calculated values of equilibrium lattice constant ( $a$ ), the three independent elastic constant ( $C_{11}$ ,  $C_{21}$ ,  $C_{44}$ ), total formation energy ( $\Delta E_f$ ) per formula unit, mechanical stability and magnetic moments ( $\mu_B$ ) per formula unit of  $M_4N$  compounds. The lattice constant was calculated using  $V = a^3$ , where  $V$  is the volume of the conventional cell of cubic  $M_4N$ . The calculated lattice constants decrease with the increase of group number until group 8 and then increase. This trend follows for each period except for 3d with  $Fe_4N$  as an exception. Formation energy is the difference between the energy of the compound and the energies of its constituent atoms in their ground states. Formation energy per formula unit of  $M_4N$  is defined as  $\Delta E_f = E(M_4N) - 4E(M) - E(N_2)/2$ , where  $E(M_4N)$  is the total energy of the solid  $M_4N$  per formula unit,  $E(M)$  is the total energy per atom of metal and  $E(N_2)$  the total energy of a nitrogen dimer. Their values for all 28  $M_4N$ s are plotted as a function of group number for 3d, 4d and 5d rows in Fig. 2. Among 28 phases of  $M_4N$ s,  $Ir_4N$  (4.02 eV) has the highest value of calculated formation energy, signifying metastability, while  $Ti_4N$  (−3.69 eV) has the lowest value suggesting high thermodynamic stability. Obviously,  $Mn_4N$  and  $Fe_4N$ , which have been experimentally synthesized are also energetically stable as their formation energies are −1.47 eV and −2.09 eV respectively per formula unit.

For mechanical stability of the cubic structures, the three elastic constants should satisfy the following criteria [98,99]:

$$C_{11} > C_{12}, C_{11} + 2C_{12} > 0, C_{44} > 0 \quad (10)$$

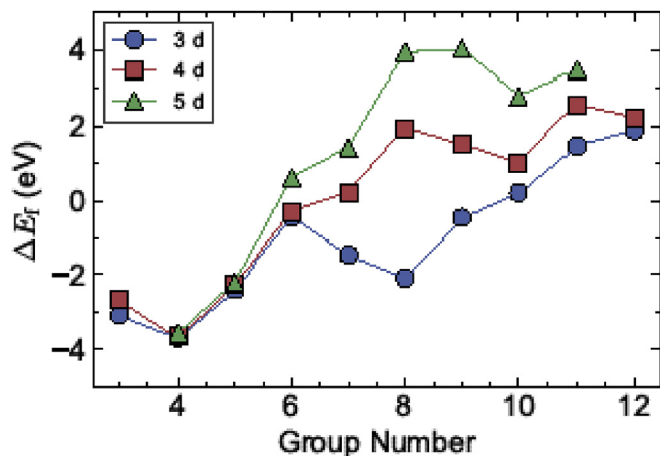
In our study, only three compounds  $V_4N$ ,  $Nb_4N$  and  $Pt_4N$  were found to be mechanically unstable (denoted as “U” in Table 3) as they did not satisfy these mechanical stability criteria of Eq. (10), while all others were mechanically stable. Mechanical stability of these compounds suggests that there's the possibility of the experimental synthesis of  $M_4N$  compounds.

Table 4 lists mechanical properties like bulk modulus ( $B$ ), shear modulus ( $G$ ), Young's modulus ( $E$ ), Pugh's ratio ( $k$ ), Poisson's ratio ( $\nu$ ), Vicker's hardness ( $H_v$ ) of the mechanically stable phases, which were calculated from our computed three fundamental elastic constants  $C_{11}$ ,  $C_{12}$ ,  $C_{44}$ . The calculated Debye temperature ( $\theta_D$ ) for all 28  $M_4N$  compounds are also listed in the table. To explore for any better trends across the periodic table, the plots of volume ( $V$ ) and bulk modulus ( $B$ )

**Table 3**

Group Number, lattice constant ( $a$ ), elastic constants ( $C_{11}$ ,  $C_{12}$ ,  $C_{44}$ ), total formation energy per formula unit ( $\Delta E_f$ ), mechanical stability (Mech. Stab.) and total magnetic moments (Mag.) in Bohr magnetons ( $\mu_B$ ) per formula unit of the nitrides  $M_4N$  of transition metals M. Stable compounds are denoted as “S” and unstable ones as “U”.

Group Number	M	$a$ (Å)	$C_{11}$ (GPa)	$C_{12}$ (GPa)	$C_{44}$ (GPa)	$\Delta E_f$ (eV)	Mech. Stab.	Mag. ( $\mu_B$ )
3	Sc	4.58	111.2	70.3	49.9	-3.09	S	1.52
4	Ti	4.17	255.5	109	88.9	-3.69	S	0
5	V	3.93	266.8	207.3	-11.9	-2.4	U	0
6	Cr	3.77	529.8	148.8	60.4	-0.44	S	0
7	Mn	3.74	452.7	103.3	120.4	-1.47	S	1.19
8	Fe	3.8	305.9	140.7	44.6	-2.09	S	9.84
9	Co	3.72	401.3	133.2	82.1	-0.46	S	6.36
10	Ni	3.73	354.2	131.7	44.4	0.21	S	1.49
11	Cu	3.88	216.2	96.3	34.9	1.46	S	0
12	Zn	4.18	91.7	81	18.6	1.88	S	0
3	Y	4.98	87.7	55.5	39.7	-2.67	S	0
4	Zr	4.56	208.6	97.9	86.5	-3.67	S	0
5	Nb	4.3	225.1	203	-20.9	-2.25	U	0
6	Mo	4.11	518.1	160	79.8	-0.29	S	0
7	Tc	4.01	597.4	166	171.5	0.22	S	0
8	Ru	3.99	532.7	173.9	117.1	1.94	S	0
9	Rh	4.03	382.3	170.4	53.6	1.5	S	0
10	Pd	4.12	246.3	146.3	34	1.02	S	0
11	Ag	4.37	148	63.1	19.2	2.57	S	0
12	Cd	4.69	70.3	53.9	10.7	2.22	S	0
4	Hf	4.51	231	104.2	97.6	-3.58	S	0
5	Ta	4.29	285.7	218.2	21.5	-2.22	S	0
6	W	4.14	549.8	210	46	0.62	S	0
7	Re	4.05	711.5	202.5	209.3	1.42	S	0
8	Os	4.03	642.4	222.7	138.8	3.94	S	0
9	Ir	4.07	467.1	219.5	41.8	4.02	S	0
10	Pt	4.17	302.3	195.2	-3.2	2.79	U	0
11	Au	4.38	158.3	105.8	3.4	3.47	S	0



**Fig. 2.** Total formation energy per formula unit ( $\Delta E_f$ ) of the nitrides  $M_4N$  versus group number of their corresponding transition metals (M). Blue circles, red squares and green triangle represent the corresponding nitrides of metals in the 3d, 4d and 5d rows respectively. For example, group number 4 stands for Ti (blue circle), Zr (red square), and Hf (green triangle). (For interpretation of the references to colour in this figure legend, the reader is referred to the Web version of this article.)

of  $M_4N$  as a function of the group number for 3d, 4d and 5d rows of transition metals are drawn in Fig. 3. We can see a trend that the volume decreases first until group 8 and then increases thereafter for 4d and 5d rows, but the trend deviates slightly for the 3d row. Similarly, values of Bulk modulus increase first with group number and peak at group 7 and then decrease further for 4d and 5d rows, while this trend doesn't follow completely for the 3d row. From the trend in  $V$  and  $B$  for 4d and 5d rows, an anti-correlation can be observed between  $V$  and  $B$  among  $M_4N$ s. Hard coatings applications require materials with high hardness and the hardness of materials is measured in terms of Vickers

**Table 4**

Group Number, Bulk modulus ( $B$ ), polycrystalline shear modulus ( $G$ ), Young's modulus ( $E$ ), Pugh's ratio ( $k$ ), Poisson's ratio ( $\nu$ ), Vickers hardness ( $H_V$ ) and Debye temperature ( $\theta_D$ ) of nitrides  $M_4N$  of transition metals M. Mechanically unstable compounds are denoted as “U” without a numerical value.

Group Number	M	$B$ (GPa)	$G$ (GPa)	$E$ (GPa)	$k$	$\nu$	$H_V$ (GPa)	$\theta_D$ (K)
3	Sc	83.9	34.9	91.9	0.42	0.32	4.2	400.5
4	Ti	157.8	82.2	210.2	0.52	0.28	10	567.3
5	V	U	U	U	U	U	U	U
6	Cr	275.8	97.8	262.3	0.35	0.34	7.3	570.7
7	Mn	219.8	139.8	346.1	0.64	0.24	18.2	654.0
8	Fe	195.8	57.2	156.4	0.29	0.37	4.0	424.9
9	Co	222.6	100.0	260.9	0.45	0.30	9.7	537.8
10	Ni	205.9	64.8	175.9	0.31	0.36	4.7	437.3
11	Cu	136.3	43.4	117.7	0.32	0.36	3.6	351.4
12	Zn	84.6	11.3	32.5	0.13	0.44	0.5	185.9
3	Y	66.3	27.6	72.8	0.42	0.32	3.6	269.1
4	Zr	134.8	72.4	184.1	0.54	0.27	9.4	409.6
5	Nb	U	U	U	U	U	U	U
6	Mo	279.3	111.0	294.1	0.40	0.32	9.0	473.3
7	Tc	309.8	188.0	469.1	0.61	0.25	21.2	596.3
8	Ru	293.5	139.0	360.2	0.47	0.30	12.9	506.6
9	Rh	241.0	70.7	193.2	0.29	0.37	4.7	363.4
10	Pd	179.6	39.7	110.9	0.22	0.40	2.2	272.1
11	Ag	91.4	26.5	72.5	0.29	0.37	2.3	226.5
12	Cd	59.4	9.6	27.3	0.16	0.42	0.6	139.5
4	Hf	146.5	82.1	207.4	0.56	0.26	10.8	312.4
5	Ta	240.7	25.7	74.6	0.11	0.45	0.7	173.7
6	W	323.3	80.3	222.4	0.25	0.39	4.2	296.6
7	Re	372.1	226.3	564.5	0.61	0.25	24.3	480.8
8	Os	362.6	163.9	427.2	0.45	0.30	13.8	406.4
9	Ir	302.0	65.8	184.0	0.22	0.40	3.1	261.0
10	Pt	U	U	U	U	U	U	U
11	Au	123.3	8.9	25.9	0.07	0.46	0.2	99.0

hardness ( $H_V$ ). In this paper, we have used the theoretically modeled formulation of Tian et al. [85] for hardness calculation. From our calculation, The nitrides of Group 7,  $Mn_4N$ ,  $Tc_4N$  and  $Re_4N$  were found to

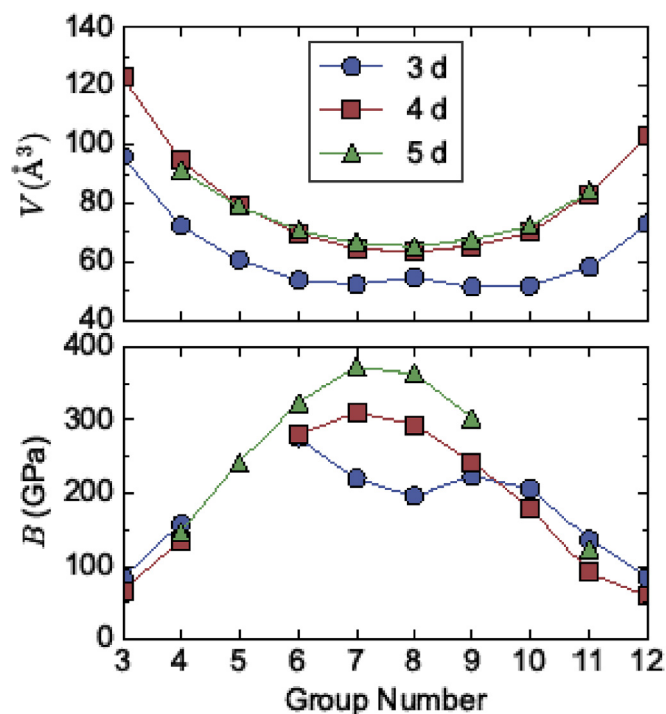


Fig. 3. Computed equilibrium volume ( $V$ ) and bulk modulus ( $B$ ) of the nitrides  $M_4N$  versus the group number of their corresponding transition metals ( $M$ ). Blue circles, red squares and green triangle represent the corresponding nitrides of metals in the 3 d, 4 d, and 5 d rows respectively. Data have not been shown for unstable nitrides leading to breaks in the lines, which are only a guide to the eye. (For interpretation of the references to colour in this figure legend, the reader is referred to the Web version of this article.)

be the hardest compounds with Vickers hardness of 18.2 GPa, 21.2 GPa, and 24.3 GPa respectively. Our values of  $H_V$  for these three compounds compare well with the values for the most commonly used hard material rocksalt-structured TiN, measured by Shin et al. [22] (20.2 GPa) using ultra-high vacuum dc magnetron sputter deposition and value provided by Holleck [7] (21 GPa). These three compounds also compete with pyrite-type hard compounds  $PtN_2$  (23.5 GPa) and  $MnN_2$  (19.9 GPa) reported previously by Liu et al. [78]. Nitrides of Group 4 ( $Ti_4N$ ,  $Zr_4N$ ,  $Hf_4N$ ) and Group 8 ( $Ru_4N$ ,  $Os_4N$ ) also have  $H_V$  around or above 10 GPa.  $Co_4N$  is the hardest compound in group 9 with  $H_V$  of 9.7 GPa. The elastic constant  $C_{44}$  signifies material's stability against shear deformations [4,50,64,65] and  $G$  is the material's ability to oppose shear strain. As the hard nitrides of Re, Tc, and Mn of group 7 possess not only the higher values of  $C_{44}$  but also larger shear modulus ( $G$ ), they are very stable against any kind of shear deformation. A common trend of  $M_4N$  compounds in  $H_V$ ,  $k$ , and  $G$ , as illustrated in the plots of Fig. 4 also supports this fact. From Table 1, since  $Au_4N$  has a  $C_{44}$  value of only 3.4 GPa, it should be considered marginally stable. Based on the results of our investigation, experimentalists will have an opportunity to narrow their search for an experimental synthesis of these nitrides, by eliminating 3 unstable and other relatively soft phases and focusing attention to the 3 predicted hard phases, saving huge experimental effort. The brittle to the ductile behavior of materials is indicated by the values of Pugh's ratio ( $k = G/B$ ) and Cauchy pressure ( $P_C = C_{12} - C_{44}$ ) [102–106]. The condition for material's ductility as given by Pettifor [106] and Pugh [105] is  $P_C \geq 0$  and  $k \leq 0.57$ . With this condition, we observe that all our  $M_4N$  compounds possess ductile nature except  $Mn_4N$ ,  $Tc_4N$ , and  $Re_4N$ . Therefore, unlike the tough materials reported by Sangiovanni et al. [107,108], these three are hard and brittle. But there are other two ductile candidates  $Ru_4N$  and  $Os_4N$  with a modest hardness of 12.9 GPa and 13.8 GPa respectively and may be considered as moderately tough materials.

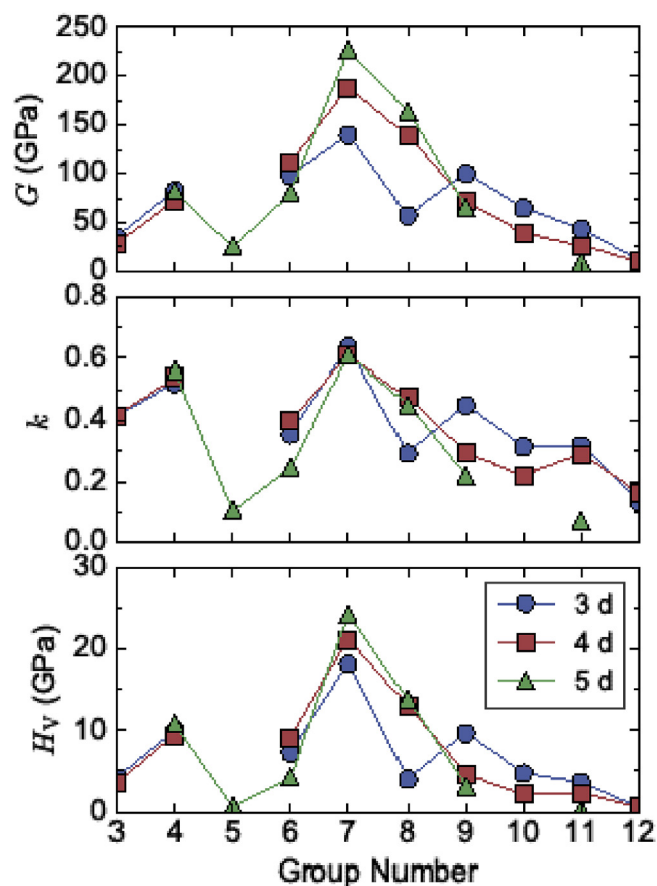


Fig. 4. Polycrystalline shear modulus ( $G$ ), Pugh's ratio ( $k$ ) and Vickers Hardness ( $H_V$ ) of the nitrides  $M_4N$  versus group number of their corresponding transition metals ( $M$ ). Blue circles, red squares and green triangle represent the corresponding nitrides of metals in the 3 d, 4 d, and 5 d rows respectively. Data have not been shown for unstable nitrides leading to breaks in the lines, which are only a guide to the eye. (For interpretation of the references to colour in this figure legend, the reader is referred to the Web version of this article.)

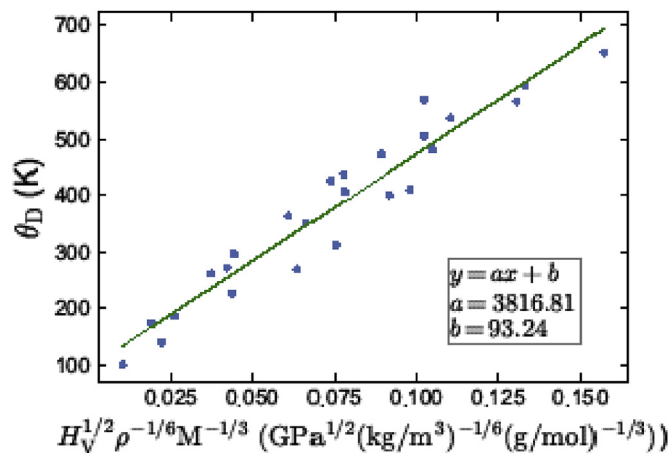


Fig. 5. Computed Debye temperature ( $\theta_D$ ) from equation (6) versus Vickers hardness ( $H_V$ ) from Eq. (5). Symbols are data points which have been shown only for mechanically stable compounds. The line is a linear fit to Eq. (9).

Our calculations of Debye temperature ( $\theta_D$ ) indicate that 9 compounds  $Zn_4N$ ,  $Y_4N$ ,  $Pd_4N$ ,  $Ag_4N$ ,  $Cd_4N$ ,  $Ta_4N$ ,  $W_4N$ ,  $Ir_4N$ , and  $Au_4N$  were found to possess  $\theta_D$  less than 300 K. These are the compounds with relatively low Vickers hardness. Fig. 5 shows a linear correlation between  $\theta_D$  calculated from Eq. (6) with hardness ( $H_V$ ) calculated from

Eq. (5) indicating that compounds with high  $H_V$  also possess high  $\theta_D$ . Similar linear correlations have been found by Deus [86] for diamond-like semiconducting compounds and by Miao et al. [104] for Ta<sub>3</sub>B<sub>4</sub>-structured transition metal borides. Moreover, Debye temperature is also correlated with the melting point ( $T_m$ ) given by Lindemann [109] as  $\theta_D = \alpha \times T_m^{1/2} M^{-1/2} V^{-1/3}$ . For better performance in hard coatings, materials with not only high hardness but also with high melting points are preferred because such materials can be used in a wide range of temperature. The adherence of our data to a fit of this equation suggests that M<sub>4</sub>N materials with large hardness will also have a high melting point due to bonding strength. Such type of hard materials can be of use in high temperature applications.

### 3.2. Magnetic properties

From our DFT calculations, five mechanically stable M<sub>4</sub>N compounds, namely Sc<sub>4</sub>N (1.52  $\mu_B$ ), Mn<sub>4</sub>N (1.19  $\mu_B$ ), Fe<sub>4</sub>N (9.84  $\mu_B$ ), Co<sub>4</sub>N (6.36  $\mu_B$ ), and Ni<sub>4</sub>N (1.49  $\mu_B$ ) are observed to have non-zero magnetic moments while the rest have zero magnetic moments. However, Cr<sub>4</sub>N is found to have a total zero magnetic moment with each of its atom in the unit cell possessing a zero-magnetic moment. This is unlike the elemental Cr, which has an antiferromagnetic ordering. We performed the structural energy minimization of Cr<sub>4</sub>N with an initial guess of antiferromagnetic spin sets (1, -1, 1, -1, 0) and Cr<sub>4</sub>N was found to be stabilized in its lowest ground state with a total of zero magnetic moment while the individual local moments of its constituents also being zero. These magnetic compounds are in the 3d period of the periodic table. From our calculation of magnetic moments due to electronic spin-polarization, Mn<sub>4</sub>N was found to be ferrimagnetic with a total magnetic moment of 1.19  $\mu_B$ , where all of the face-centered atomic moments align antiparallel to the corner atomic moment. The Fe<sub>4</sub>N phase was found to be ferromagnetic with a total magnetic moment of 9.84  $\mu_B$ , where all the atomic moments are aligned parallel to each other. Similarly, Co<sub>4</sub>N, Ni<sub>4</sub>N, and Sc<sub>4</sub>N were also found to have a ferromagnetic ordering. The calculated magnetic moments due to the electrons in s, p and d orbitals along with the magnetic moments of individual atoms for these magnetic compounds are provided in Table S1 of the Supplemental Material. A clear agreement between experimental and calculated values for the lattice constants and magnetic moments can be observed from Table 2 for two experimentally explored magnetic compounds Mn<sub>4</sub>N and Fe<sub>4</sub>N.

We are primarily focused on mechanical properties like hardness. This focus necessitates that at least a preliminary modeling of magnetism in DFT calculations is required as it may significantly affect these properties. Many DFT calculations in the past have ignored magnetism caused by electronic spin-polarization [53–55,110–112]. However, the mechanical properties of materials like B1-type CrN can be explained only when magnetism is taken into account [34,64–66,87,113–115]. The paramagnetic phase above room temperature should be simulated by a construction of randomized magnetic spins, rather than a non-magnetic model to obtain the correct energy and elastic constants [34,87,113–115]. On the other hand, differences in energy and mechanical properties arising from differences in magnetic orderings, i.e. ferromagnetic, anti-ferromagnetic, or paramagnetic, are smaller than those between magnetic and non-magnetic simulations [34,87,113–115]. Therefore, in this work, we included magnetism for all the compounds we studied and compared with the results of non-magnetic calculations. Table 5 lists a comparison between the properties of magnetic phases calculated by considering the structure with magnetic configurations and with non-magnetic configurations. The inclusion of magnetism has affected the values of lattice constants and elastic constants and hence those of other derived moduli significantly, which can be observed distinctly from Table 5. The influence of magnetism on the hardness of M<sub>4</sub>N-type metal nitrides can be seen on the reduction of the hardness of Mn<sub>4</sub>N and Fe<sub>4</sub>N. With non-magnetic configuration, Mn<sub>4</sub>N is a hard material with an  $H_V$  of

20.8 GPa, along with Tc<sub>4</sub>N and Re<sub>4</sub>N in the same Group 7, but when ferrimagnetic configuration is considered for Mn<sub>4</sub>N with initial guess for magnetic moments of 3.5  $\mu_B$  for the corner and -0.7  $\mu_B$  for the face-centered atoms,  $H_V$  reduces to 18.2 GPa. More notably, the hardness of Fe<sub>4</sub>N decreases from 12.4 GPa to 4.0 GPa under the consideration of ferromagnetic configuration with an initial guess for magnetic moments of 3  $\mu_B$  for the corner and 2  $\mu_B$  for the face-centered atoms. On the other hand, the hardness of Sc<sub>4</sub>N, Co<sub>4</sub>N, and Ni<sub>4</sub>N increase under magnetic configuration treatment. Thus, proper consideration of magnetism is deemed to be essential in these magnetic compounds to compute correct values of various mechanical properties such as hardness.

### 3.3. Electronic structure

Table 6 and Fig. 6 show electronegativity ( $\chi$ ) and Bader charge transfer ( $q_{\text{trans}}$ ) of the 28 M<sub>4</sub>N-type metal nitrides. The values of  $\chi$  for metals were taken from the literature [116]. The electronegativity ( $\chi$ ) of metals and charge transferred from metals to nitrogen are anti-correlated as expected. No correlation between the charge transfer and electronegativity with the hardness was found.

We computed the electronic total density of states (TDOS) for all 28 M<sub>4</sub>N-type metal nitrides. The calculated TDOS for 10 3d M<sub>4</sub>N compounds are displayed in Fig. 7. Since there are states around the Fermi energy ( $E_F$ ) level; we could see no gap between the valence and the conduction band in 3d M<sub>4</sub>N-type metal nitrides. Similarly, no energy band gaps were found in the case of 4d and 5d rows M<sub>4</sub>N-type metal nitrides as observed from the Figs. S1 and S2 of the Supplemental Material. This means all 28 M<sub>4</sub>N-type metal nitrides are metallic in nature and which is reasonable since the compounds are metal-rich. Additionally, as the atomic number of corresponding transition metals increases, more states tend to aggregate below the Fermi level, which is characterized by the shifting of peaks towards the left in the TDOS plots. Fig. 8 shows the plots of LDOS as a function of energy for M<sub>4</sub>N-type nitrides of group 7 (Mn<sub>4</sub>N, Tc<sub>4</sub>N, and Re<sub>4</sub>N), which are the hardest nitrides among all 28 compounds. The hybridization of nitrogen 2p orbitals with the metallic d orbital was observed due to the overlapping of the orbitals well below the Fermi level in the energy window of (-5.7, -8.6) eV for Mn<sub>4</sub>N, of (-6, -9.3) eV for Tc<sub>4</sub>N and of (-7, -10.5) eV for Re<sub>4</sub>N. The consequence of such hybridization is the strengthening of the M-N bonds thereby, contributing to the hardness of these compounds. The LDOS of group 4 M<sub>4</sub>Ns (Ti<sub>4</sub>N, Zr<sub>4</sub>N, and Hf<sub>4</sub>N), and group 11 M<sub>4</sub>Ns (Cu<sub>4</sub>N, Ag<sub>4</sub>N, and Au<sub>4</sub>N) are also appended as Figs. S3 and S4 in the Supplemental Material for comparison. From Figs. S3 and S4, it is observed that the metal d states of these group 4 and group 11 nitrides spread in a relatively narrow energy window below their Fermi level as compared to that of hard phases Mn<sub>4</sub>N, Tc<sub>4</sub>N, and Re<sub>4</sub>N. Also, relatively less extent of hybridization in metal d and nitrogen p orbitals was observed in group 4 and group 11 nitrides indicating their lesser mechanical strength. We computed the phonon density of states (DOS) for Mn<sub>4</sub>N, the experimentally synthesized stable and hard magnetic compound, as well as for V<sub>4</sub>N, the mechanically unstable compound. Their plots are shown in Fig. 9. These plots show that Mn<sub>4</sub>N has all its phonon states in the positive frequency range, which signifies that Mn<sub>4</sub>N is dynamically stabilized due to its magnetic ordering. In contrast, V<sub>4</sub>N has some of its phonon states spreading in the negative frequency range signifying its dynamical instability. The fact that Mn<sub>4</sub>N is stabilized dynamically due to its magnetic ordering is also supported by the spin-dependent density of states shown in Fig. 10 for two magnetic phases Mn<sub>4</sub>N and Fe<sub>4</sub>N. The up and down spins-states for Mn<sub>4</sub>N are distributed symmetrically with each other and the spin-states of N p orbitals hybridize perfectly with corresponding spin-states of metal d orbitals. However, the spin-dependent DOS of another magnetic compound Fe<sub>4</sub>N lacks such pattern of spin hybridization. This corresponds well with the small value (4 GPa) of Vicker's hardness of Fe<sub>4</sub>N. Additionally, its hardness decreases from 12.2 GPa to 4 GPa under the consideration of electronic spin-polarization while calculating its elastic

**Table 5**

A comparison between properties calculated with magnetic configuration (without parenthesis) and non-magnetic configurations (with parenthesis) for four magnetic  $M_4N$ -type compounds. The symbols in bold represent the properties listed in Tables 3 and 4

$M_4N$	$a$ (Å)	$C_{11}$ (GPa)	$C_{12}$ (GPa)	$C_{44}$ (GPa)	Mag. ( $\mu_B$ )	$B$ (GPa)	$G$ (GPa)	$E$ (GPa)	$k$	$\nu$	$H_v$ (GPa)
$Sc_4N$	4.58	111.2	70.3	49.9	1.52	83.9	34.9	91.9	0.42	0.32	4.2
	(4.57)	(107.1)	(74.4)	(46.5)	(0.00)	(85.3)	(30.6)	(82.0)	(0.36)	(0.34)	(3.2)
$Mn_4N$	3.74	452.7	103.3	120.4	1.19	219.8	139.8	346.1	0.64	0.24	18.2
	(3.69)	(602.9)	(134.1)	(149.0)	(0.00)	(290.4)	(178.8)	(445.0)	(0.62)	(0.24)	(20.8)
$Fe_4N$	3.80	305.9	140.7	44.6	9.94	195.8	57.2	156.4	0.29	0.37	4.0
	(3.67)	(525.4)	(154.9)	(103.9)	(0.00)	(278.4)	(131.3)	(340.3)	(0.47)	(0.30)	(12.4)
$Co_4N$	3.72	401.3	133.2	82.1	6.36	222.6	100.0	260.9	0.45	0.30	9.7
	(3.68)	(428.6)	(160.6)	(72.0)	(0.00)	(249.9)	(92.6)	(247.2)	(0.37)	(0.34)	(7.3)
$Ni_4N$	3.73	354.2	131.7	44.4	1.49	205.9	64.8	175.9	0.31	0.36	4.7
	(3.73)	(355.7)	(139.0)	(33.6)	(0.00)	(211.2)	(54.9)	(151.6)	(0.26)	(0.38)	(3.4)

**Table 6**

Electronegativity ( $\chi$ ) [116] of the transition metals (M) and Bader charge transfer ( $q_{trans}$ ) from metal (M) atoms to one nitrogen (N) atom in  $M_4N$ -type metal nitrides.

Group Number	M	$\chi$	$q_{trans}$
3	Sc Y	N/A	1.2 1.11 N/A
4	Ti Zr Hf	1.32 1.22 1.23	2.03 1.96 1.97
5	V Nb Ta	1.45 1.23 1.33	1.83 1.81 1.86
6	Cr Mo W	1.56 1.3 1.4	1.6 1.56 1.7
7	Mn Tc Re	1.6 1.36 1.46	1.48 1.39 1.39
8	Fe Ru Os	1.64 1.42 1.52	1.26 1.15 1.28
9	Co Rh Ir	1.7 1.45 1.55	1.15 0.97 1.08
10	Ni Pd Pt	1.75 1.35 1.44	1.14 0.83 0.93
11	Cu Ag Au	1.75 1.42 1.42	1.21 0.97 0.85
12	Zn Cd	N/A	1.66 1.46 N/A

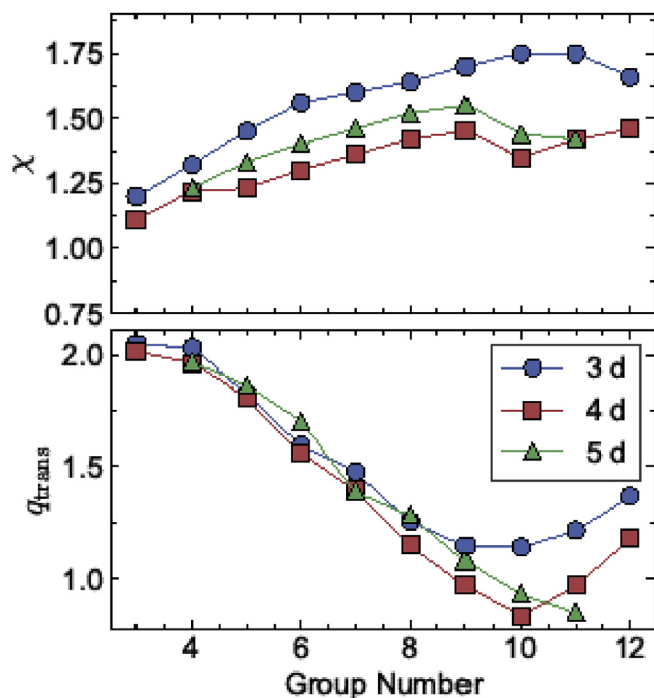


**Fig. 6.** Electronegativity ( $\chi$ ) of the transition metals (M) and Bader charge transfer from metal (M) atoms to nitrogen (N) atoms ( $q_{trans}$ ) in  $M_4N$ -type metal nitrides of the 3 d, 4 d, and 5 d metals. Blue circles, red squares and green triangle represent the corresponding nitrides of metals in the 3 d, 4 d, and 5 d rows respectively. The data in the two panels suggests anti-correlation of  $q_{trans}$  with  $\chi$ . (For interpretation of the references to colour in this figure legend, the reader is referred to the Web version of this article.)

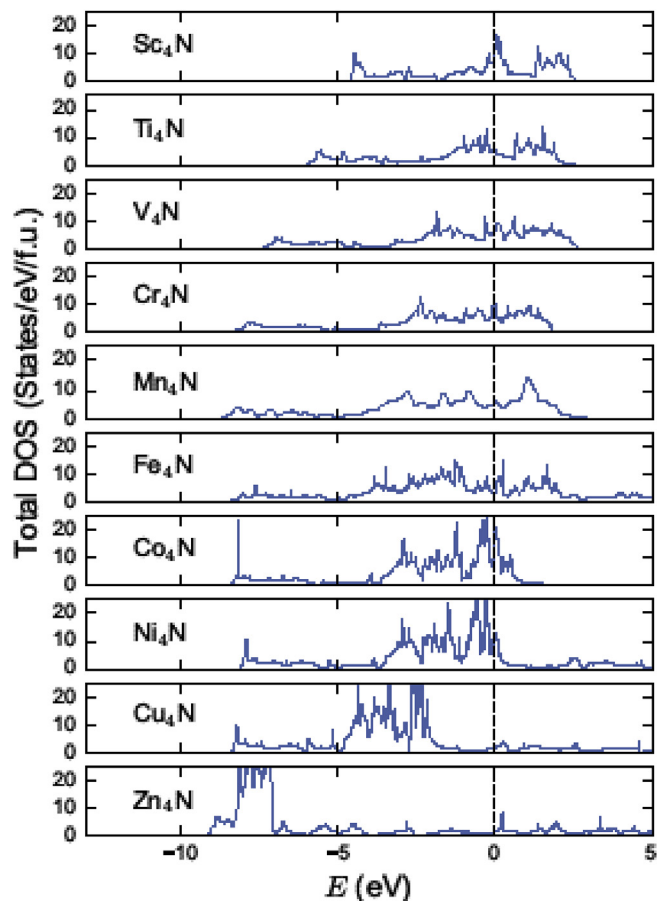


**Fig. 7.** Total Density of States (DOS) per formula unit (primitive cell) of the 10 3 d  $M_4N$ -type transition metal nitrides. Fermi energy is set to zero in each panel.

constants as mentioned earlier.

#### 4. Conclusions

In summary, we performed density functional theory based first-principles calculations on the 28 nitrides of 3 d, 4 d and 5 d transition metals in metal-rich  $M_4N$  structure. We calculated their formation energy, lattice constants, elastic constants, mechanical stability, magnetic moments, bulk modulus, shear modulus, Young's modulus, Poisson's ratio, Pugh's ratio, Vickers hardness and Debye temperature. A relatively high Vickers hardness was observed in compounds of group 7 with  $Re_4N$  (24.3 GPa) being the hardest. As seen from the calculated local density of states of  $Mn_4N$ ,  $Tc_4N$ , and  $Re_4N$ , hybridization of metal d orbital with nitrogen p orbital plays an important role in hardening the material. The effect of magnetism on mechanical properties of

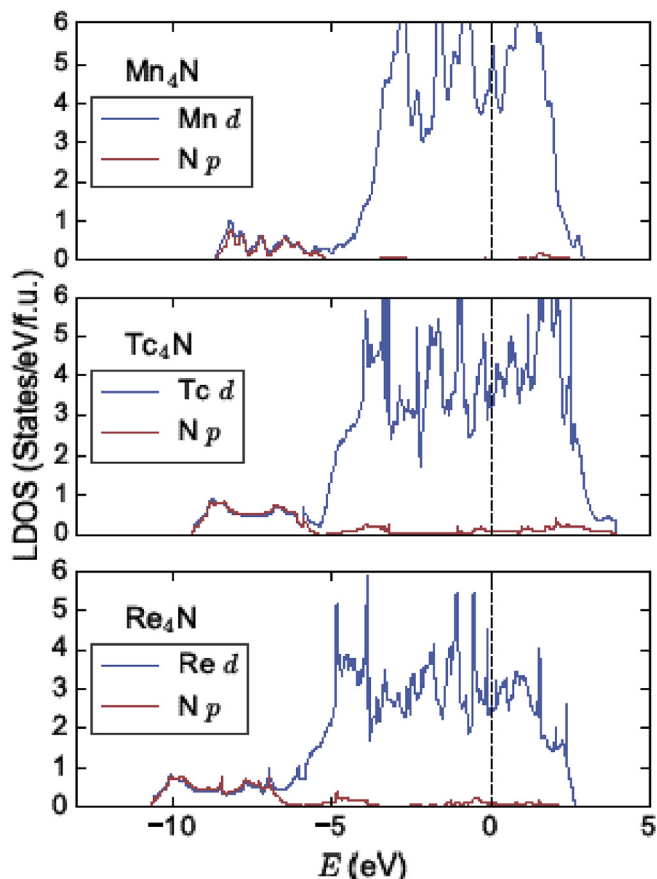


Fig. 8. Local density of states (LDOS) of  $M_4N$ -type group 7 nitrides  $Mn_4N$ ,  $Tc_4N$ , and  $Re_4N$ , which have the highest Vicker's hardness. Fermi energy is set to zero in each panel.

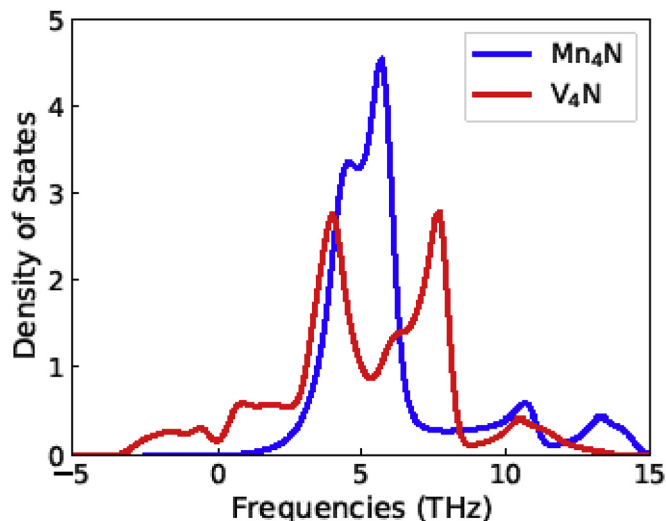


Fig. 9. Phonon density of states (DOS) for  $Mn_4N$  and  $V_4N$ .

magnetic compounds like  $Mn_4N$ ,  $Fe_4N$  etc. was observed and proved to be essential to take into consideration. Our work enriches the database for hard-coating materials based on transition metal nitrides and offers a guideline for selection of desired materials with promising physical properties while avoiding the effort for the experimental synthesis of unstable materials.

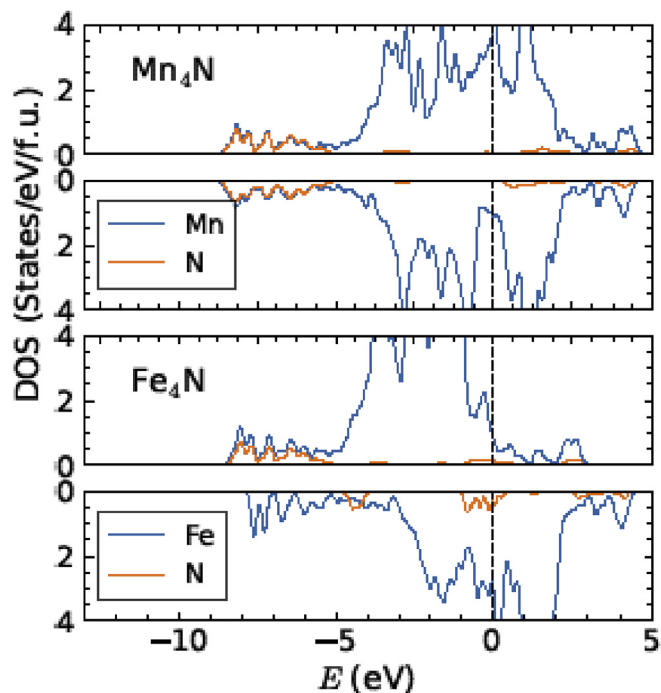


Fig. 10. The spin-dependent density of states (DOS) of magnetic phases  $Mn_4N$  (upper two panels) and  $Fe_4N$  (lower two panels). Fermi energy is set to zero in each panel. Spin-up and spin-down states are shown in the erected and inverted axis respectively.

#### Acknowledgments

The computing for this project was performed at the Tandy Supercomputing Center (TSC) [117] at Oklahoma Innovation Institute (OII) and Ohio Supercomputer Center (OSC) [118]. We thank the CMMI from the National Science Foundation grants 1629239 and 1629230 for funding this work.

#### Appendix A. Supplementary data

Supplementary data related to this article can be found at <http://dx.doi.org/10.1016/j.jpcs.2018.04.043>.

#### References

- [1] J.G. Zhao, S.J. You, L.X. Yang, C.Q. Jin, Structural phase transition of  $Cu_3N$  under high pressure, *Solid State Commun.* 150 (2010) 1521–1524, <http://dx.doi.org/10.1016/j.ssc.2010.06.012>.
- [2] S. Kodambaka, S.V. Khare, V. Petrova, D.D. Johnson, I. Petrov, J.E. Greene, Absolute orientation-dependent anisotropic TiN(111) island step energies and stiffnesses from shape fluctuation analyses, *Phys. Rev. B* 67 (2003), <http://dx.doi.org/10.1103/PhysRevB.67.035409>.
- [3] S.H. Jhi, S.G. Louie, M.L. Cohen, J. Ihm, Vacancy hardening and softening in transition metal carbides and nitrides, *Phys. Rev. Lett.* 86 (2001) 3348–3351, <http://dx.doi.org/10.1103/PhysRevLett.86.3348>.
- [4] S.H. Jhi, J. Ihm, S.G. Louie, M.L. Cohen, Electronic mechanism of hardness enhancement in transition-metal carbonitrides, *Nature* 399 (1999) 132–134, <http://dx.doi.org/10.1038/20148>.
- [5] A.Y. Liu, M.L. Cohen, Prediction of new low compressibility solids. *Science* 245 (1989) 841–842, <http://dx.doi.org/10.1126/science.245.4920.841>.
- [6] X.J. Chen, V. V. Struzhkin, Z.G. Wu, M. Somayazulu, J. Qian, S. Kung, A.N. Christensen, Y.S. Zhao, R.E. Cohen, H.K. Mao, R.J. Hemley, Hard superconducting nitrides, *Proc. Natl. Acad. Sci. U. S. A* 102 (2005) 3198–3201, <http://dx.doi.org/10.1073/pnas.0500174102>.
- [7] H. Holleck, Material selection for hard coatings, *J. Vac. Sci. Technol. A Vacuum Surfaces, Film* 4 (1986) 2661, <http://dx.doi.org/10.1116/1.573700>.
- [8] J.C. Crowhurst, Synthesis and characterization of the nitrides of platinum and iridium, *Science (Wash. D C)* 311 (2006) 1275–1278, <http://dx.doi.org/10.1126/science.1121813>.
- [9] E. Gregoryanz, C. Sanloup, M. Somayazulu, J. Badro, G. Fiquet, H.K. Mao, R.J. Hemley, Synthesis and characterization of a binary noble metal nitride, *Nat. Mater.* 3 (2004) 294–297, <http://dx.doi.org/10.1038/nmat1115>.

- [10] J.A. Montoya, A.D. Hernandez, C. Sanloup, E. Gregoryanz, S. Scandolo, OsN<sub>2</sub>: crystal structure and electronic properties, *Appl. Phys. Lett.* 90 (2007), <http://dx.doi.org/10.1063/1.2430631>.
- [11] A.F. Young, C. Sanloup, E. Gregoryanz, S. Scandolo, R.J. Hemley, H.K. Mao, Synthesis of novel transition metal nitrides IrN<sub>2</sub> and OsN<sub>2</sub>, *Phys. Rev. Lett.* 96 (2006) 1–4, <http://dx.doi.org/10.1103/PhysRevLett.96.155501>.
- [12] J.C. Crowhurst, A.F. Goncharov, B. Sadigh, J.M. Zaug, D. Aberg, Y. Meng, V.B. Prakapenka, Synthesis and characterization of nitrides of iridium and palladium, *J. Mater. Res.* 23 (2008) 1–5, <http://dx.doi.org/10.1557/jmr.2008.0027>.
- [13] J.P. Dismukes, W.M. Yim, V.S. Ban, Epitaxial growth and properties of semi-conducting ScN, *J. Cryst. Growth* 13 (1971) 365.
- [14] D. Gall, I. Petrov, N. Hellgren, L. Hultman, J.E. Sundgren, J.E. Greene, Growth of poly- and single-crystal ScN on MgO (001): role of low-energy N-2(+) irradiation in determining texture, microstructure evolution, and mechanical properties, *J. Appl. Phys.* 84 (1998) 6034–6041, <http://dx.doi.org/10.1063/1.368913>.
- [15] G. Travaglini, F. Marabelli, R. Monnier, E. Kaldis, P. Wachter, Electronic structure of ScN, *Phys. Rev. B* 34 (1986) 3876–3882, <http://dx.doi.org/10.1103/PhysRevB.34.3876>.
- [16] H.A.H. Al-Britthen, E.M. Trifan, D.C. Ingram, A.R. Smith, D. Gall, Phase stability, nitrogen vacancies, growth mode, and surface structure of ScN(001) under Sc-rich conditions, *J. Cryst. Growth* 242 (2002) 345–354, [http://dx.doi.org/10.1016/S0022-0248\(02\)01447-1](http://dx.doi.org/10.1016/S0022-0248(02)01447-1).
- [17] R.P. Deng, B.D. Ozsdolay, P.Y. Zheng, S.V. Khare, D. Gall, Optical and transport measurement and first-principles determination of the ScN band gap, *Phys. Rev. B* 91 (2015), <http://dx.doi.org/10.1103/PhysRevB.91.045104> Artn 045104.
- [18] J.P. Dismukes, W.M. Yim, J.J. Tietjen, R.E. Novak, Vapor deposition semi-conducting mononitrides of Sc, Y and rare earth elements, *J. Cryst. Growth* 9 (1971) 295, [http://dx.doi.org/10.1016/0022-0248\(71\)90244-2](http://dx.doi.org/10.1016/0022-0248(71)90244-2).
- [19] H.H. Chen, F. Peng, H.K. Mao, G.Y. Shen, H.P. Liermann, Z.O. Li, J.F. Shu, Strength and elastic moduli of TiN from radial x-ray diffraction under nonhydrostatic compression up to 45 GPa, *J. Appl. Phys.* 107 (2010), <http://dx.doi.org/10.1063/1.3392848>.
- [20] K. Liu, X.L. Zhou, H.H. Chen, L.Y. Lu, Structural and elastic properties of TiN under high pressure, *Phys. B Condens. Matter* 407 (2012) 3617–3621, <http://dx.doi.org/10.1016/j.physb.2012.05.038>.
- [21] W.J. Meng, G.L. Easley, Growth and mechanical anisotropy of TiN thin films, *Thin Solid Films* 271 (1995) 108–116, [http://dx.doi.org/10.1016/0040-6090\(95\)06875-9](http://dx.doi.org/10.1016/0040-6090(95)06875-9).
- [22] C.S. Shin, D. Gall, N. Hellgren, J. Patscheider, I. Petrov, J.E. Greene, Vacancy hardening in single-crystal TiN<sub>x</sub>(001) layers, *J. Appl. Phys.* 93 (2003) 6025–6028, <http://dx.doi.org/10.1063/1.1568521>.
- [23] M. Mattesini, R. Ahuja, B. Johansson, Cubic Hf<sub>3</sub>N<sub>4</sub> and Zr<sub>3</sub>N<sub>4</sub>: a class of hard materials, *Phys. Rev. B* 68 (2003), <http://dx.doi.org/10.1103/PhysRevB.68.184108>.
- [24] A. Zerr, N. Chigarev, R. Brenner, D.A. Dzivenko, V. Gusev, Elastic moduli of hard c-Zr<sub>3</sub>N<sub>4</sub> from laser ultrasonic measurements, *Phys. Status Solidi rapid Res. Lett.* 4 (2010) 353–355, <http://dx.doi.org/10.1002/psrr.201004345>.
- [25] D.A. Dzivenko, A. Zerr, R. Boehler, R. Riedel, Equation of state of cubic hafnium (IV) nitride having Th<sub>3</sub>P<sub>4</sub>-type structure, *Solid State Commun.* 139 (2006) 255–258, <http://dx.doi.org/10.1016/j.ssc.2006.06.020>.
- [26] O. Shebanova, E. Soignard, P.F. McMillan, Compressibilities and phonon spectra of high-hardness transition metal-nitride materials, *High Pres. Res.* 26 (2006) 87–97, <http://dx.doi.org/10.1080/08957950600765186>.
- [27] D. Dzivenko, A. Zerr, N. Guignot, M. Mezouar, R. Riedel, Compressibility of cubic vanadium mononitride, *Epl* 92 (2010), <http://dx.doi.org/10.1209/0295-5075/92/66001>.
- [28] A. Friedrich, B. Winkler, L. Bayarjargal, E.A.J. Arellano, W. Morgenroth, J. Biehler, F. Schroder, J.Y. Yan, S.M. Clark, In situ observation of the reaction of tantalum with nitrogen in a laser heated diamond anvil cell, *J. Alloy. Comp.* 502 (2010) 5–12, <http://dx.doi.org/10.1016/j.jallcom.2010.04.113>.
- [29] P. Kroll, T. Schroter, M. Peters, Prediction of novel phases of tantalum(V) nitride and tungsten(VI) nitride that can be synthesized under high pressure and high temperature, *Angew. Chemie-International Ed* 44 (2005) 4249–4254, <http://dx.doi.org/10.1002/Anie.200462980>.
- [30] E. Soignard, O. Shebanova, P.F. McMillan, Compressibility measurements and phonon spectra of hexagonal transition-metal nitrides at high pressure: epsilon-TaN, delta-Mon, and Cr<sub>2</sub>N, *Phys. Rev. B* 75 (2007), <http://dx.doi.org/10.1103/PhysRevB.75.014104>.
- [31] W.W. Lei, D. Liu, X.F. Li, J. Zhang, Q. Zhou, J.Z. Hu, Q.L. Cui, G.T. Zou, High-pressure study of low-compressibility Ta<sub>2</sub>N, *J. Physics-Condensed Matter* 19 (2007), <http://dx.doi.org/10.1088/0953-8984/19/42/425233>.
- [32] W.K. Grant, C. Loomis, J.J. Moore, D.L. Olson, B. Mishra, A.J. Perry, Characterization of hard chromium nitride coatings deposited by cathodic arc vapor deposition, *Surf. Coat. Technol.* 86 (7) (1996) 788–796, [http://dx.doi.org/10.1016/S0257-8972\(96\)03071-X](http://dx.doi.org/10.1016/S0257-8972(96)03071-X).
- [33] P. Hones, N. Martin, M. Regula, F. Levy, Structural and mechanical properties of chromium nitride, molybdenum nitride, and tungsten nitride thin films, *J. Phys. D-Applied Phys.* 36 (2003) 1023–1029, <http://dx.doi.org/10.1088/0022-3727/36/8/313>.
- [34] F. Rivadulla, M. Banobre-Lopez, C.X. Quintela, A. Pineiro, V. Pardo, D. Baldomir, M.A. Lopez-Quintela, J. Rivas, C.A. Ramos, H. Salva, J.S. Zhou, J.B. Goodenough, Reduction of the bulk modulus at high pressure in CrN, *Nat. Mater.* 8 (2009) 947–951, <http://dx.doi.org/10.1038/nmat2549>.
- [35] X.Y. Zhang, J.S. Chawla, R.P. Deng, D. Gall, Epitaxial suppression of the metal-insulator transition in CrN, *Phys. Rev. B* 84 (2011), <http://dx.doi.org/10.1103/PhysRevB.84.073101>.
- [36] M. Urgen, O.L. Eryilmaz, A.F. Cakir, E.S. Kayali, B. Nilufer, Y. Isik, Characterization of molybdenum nitride coatings produced by arc-PVD technique, *Surf. Coating. Technol.* 94 (5) (1997) 501–506, [http://dx.doi.org/10.1016/S0257-8972\(97\)00432-5](http://dx.doi.org/10.1016/S0257-8972(97)00432-5).
- [37] D. Machon, D. Daisenberger, E. Soignard, G. Shen, T. Kawashima, E. Takayama-Muromachi, P.F. McMillan, High pressure - high temperature studies and re-activity of gamma-Mo(2)N and delta-Mon, *Phys. Status Solidi a-Applications Mater. Sci.* 203 (2006) 831–836, <http://dx.doi.org/10.1002/psaa.200521008>.
- [38] E. Soignard, P.F. McMillan, T.D. Chaplin, S.M. Farag, C.L. Bull, M.S. Somayazulu, K. Leinenweber, High-pressure synthesis and study of low-compressibility molybdenum nitride (Mon and Mon<sub>(1-3)</sub>) phases, *Phys. Rev. B* 68 (2003), <http://dx.doi.org/10.1103/PhysRevB.68.132101>.
- [39] Y. Ma, Q. Cui, L. Shen, Z. He, X-ray diffraction study of nanocrystalline tungsten nitrides and tungsten to 31 GPa, *J. Appl. Phys.* 102 (2007), <http://dx.doi.org/10.1063/1.2751087>.
- [40] A. Friedrich, B. Winkler, L. Bayarjargal, W. Morgenroth, E.A. Juarez-Arellano, V. Milman, K. Refson, M. Kunz, K. Chen, Novel rhenium nitrides, *Phys. Rev. Lett.* 105 (2010), <http://dx.doi.org/10.1103/PhysRevLett.105.085504>.
- [41] A. Friedrich, B. Winkler, K. Refson, V. Milman, Vibrational properties of Re<sub>3</sub>N from experiment and theory, *Phys. Rev. B* 82 (2010), <http://dx.doi.org/10.1103/PhysRevB.82.224106>.
- [42] J.F. Adler, Q. Williams, A high-pressure X-ray diffraction study of iron nitrides: implications for Earth's core, *J. Geophys. Res. B Solid Earth* 110 (2005) 1–11, <http://dx.doi.org/10.1029/2004JB003103>.
- [43] D. Aberg, P. Erhart, J. Crowhurst, J.M. Zaug, A.F. Goncharov, B. Sadigh, Pressure-induced phase transition in the electronic structure of palladium nitride, *Phys. Rev. B* 82 (2010), <http://dx.doi.org/10.1103/PhysRevB.82.104116>.
- [44] Y.V. Butenko, L. Alves, A.C. Brievea, J. Yang, S. Krishnamurthy, L. Siller, X-ray induced decomposition of gold nitride, *Chem. Phys. Lett.* 430 (2006) 89–92, <http://dx.doi.org/10.1016/j.cplett.2006.08.096>.
- [45] L. Siller, M.R.C. Hunt, J.W. Brown, J.M. Coquel, P. Rudolf, Nitrogen ion irradiation of Au(110): formation of gold nitride, *Surf. Sci.* 513 (2002) 78–82, [http://dx.doi.org/10.1016/S0039-6028\(02\)01150-0](http://dx.doi.org/10.1016/S0039-6028(02)01150-0).
- [46] L. Siller, N. Peltekis, S. Krishnamurthy, Y. Chao, S.J. Bull, M.R.C. Hunt, Gold film with gold nitride - a conductor but harder than gold, *Appl. Phys. Lett.* 86 (2005), <http://dx.doi.org/10.1063/1.1941471>.
- [47] S. Krishnamurthy, M. Montalti, M.G. Wardle, M.J. Shaw, P.R. Briddon, K. Svensson, M.R.C. Hunt, L. Siller, Nitrogen ion irradiation of Au(110): photo-emission spectroscopy and possible crystal structures of gold nitride, *Phys. Rev. B* 70 (2004), <http://dx.doi.org/10.1103/PhysRevB.70.045414>.
- [48] J.G. Zhao, L.X. Yang, S.J. You, F.Y. Li, C.Q. Jin, J. Liu, Structural stability of Zn<sub>3</sub>N<sub>2</sub> under high pressure, *Phys. B Condens. Matter* 405 (2010) 1836–1838, <http://dx.doi.org/10.1016/j.physb.2010.01.057>.
- [49] S.K.R. Patil, S.V. Khare, B.R. Tuttle, J.K. Bording, S. Kodambaka, Mechanical stability of possible structures of PtN investigated using first-principles calculations, *Phys. Rev. B Condens. Matter* 73 (2006) 1–8, <http://dx.doi.org/10.1103/PhysRevB.73.104118>.
- [50] S.K.R. Patil, N.S. Mangale, S.V. Khare, S. Marsillac, Super hard cubic phases of period VI transition metal nitrides: first principles investigation, *Thin Solid Films* 517 (2008) 824–827, <http://dx.doi.org/10.1016/j.tsf.2008.07.034>.
- [51] W. Chen, J.Z. Jiang, Elastic properties and electronic structures of 4d- and 5d-transition metal mononitrides, *J. Alloy. Comp.* 499 (2010) 243–254, <http://dx.doi.org/10.1016/j.jallcom.2010.03.176>.
- [52] E.J. Zhao, J.P. Wang, J. Meng, Z.J. Wu, Structural, mechanical and electronic properties of 4d transition metal mononitrides by first-principles, *Comput. Mater. Sci.* 47 (2010) 1064–1071, <http://dx.doi.org/10.1016/j.commatsci.2009.12.011>.
- [53] Z.T.Y. Liu, X. Zhou, S.V. Khare, D. Gall, Structural, mechanical and electronic properties of 3d transition metal nitrides in cubic zincblende and cesium chloride structures: a first-principles investigation, *J. Phys. Condens. Matter* 26 (2014) 25404, <http://dx.doi.org/10.1088/0953-8984/26/2/025404>.
- [54] Z.T.Y. Liu, X. Zhou, D. Gall, S.V. Khare, First-principles investigation of the structural, mechanical and electronic properties of the NbO-structured 3d, 4d and 5d transition metal nitrides, *Comput. Mater. Sci.* 84 (2014) 365–373, <http://dx.doi.org/10.1016/j.commatsci.2013.12.038>.
- [55] X. Zhou, D. Gall, S.V. Khare, Mechanical properties and electronic structure of anti-ReO<sub>3</sub> structured cubic nitrides, M<sub>3</sub>N, of d block transition metals M: an ab initio study, *J. Alloy. Comp.* 595 (2014) 80–86, <http://dx.doi.org/10.1016/j.jallcom.2014.01.116>.
- [56] W.J. Takei, G. Shirane, B.C. Frazer, Magnetic structure of Mn<sub>4</sub>N, *Phys. Rev.* 119 (1960) 122–126, <http://dx.doi.org/10.1103/PhysRev.119.122>.
- [57] M. Mekata, Magnetic study on Mn<sub>4</sub>N and its related compounds, *J. Phys. Soc. Japan* 17 (1962) 796.
- [58] B.C. Frazer, Magnetic structure of Fe<sub>4</sub>N, *Phys. Rev.* 112 (1958) 751–754, <http://dx.doi.org/10.1103/PhysRev.112.751>.
- [59] Z.Q. Lv, Y. Gao, S.H. Sun, M.G. Qv, Z.H. Wang, Z.P. Shi, W.T. Fu, Electronic, magnetic and elastic properties of gamma-Fe<sub>4</sub>X (X=B/C/N) from density functional theory calculations, *J. Magn. Magn. Mater.* 333 (2013) 39–45, <http://dx.doi.org/10.1016/J.Jmmm.2012.12.044>.
- [60] J. von Appen, R. Dronskowski, Predicting new ferromagnetic nitrides from electronic structure theory: IrFe<sub>3</sub>N and RhFe<sub>3</sub>N, *Angew. Chemie-International Ed* 44 (2005) 1205–1210, <http://dx.doi.org/10.1002/Anie.200462247>.
- [61] D. Music, J.M. Schneider, Elastic properties of MFe<sub>3</sub>N (M=Ni, Pd, Pt) studied by ab initio calculations, *Appl. Phys. Lett.* 88 (2006) 3, <http://dx.doi.org/10.1063/1.2165285>.
- [62] T. Takahashi, J. Burghaus, D. Music, R. Dronskowski, J.M. Schneider, Elastic properties of gamma-Fe<sub>4</sub>N probed by nanoindentation and ab initio calculation,

- Acta Mater. 60 (2012) 2054–2060, <http://dx.doi.org/10.1016/j.actamat.2011.12.051>.
- [63] A. Houben, P. Muller, J. von Appen, H. Lueken, R. Niewa, R. Dronskowski, Synthesis, crystal structure, and magnetic properties of the semihard itinerant ferromagnet RhFe<sub>3</sub>N, *Angew. Chemie-International Ed* 44 (2005) 7212–7215, <http://dx.doi.org/10.1002/anie.200502579>.
- [64] G. Kresse, J. Furthmuller, Efficient iterative schemes for ab initio total-energy calculations using a plane-wave basis set, *Phys. Rev. B* 54 (1996) 11169–11186, <http://dx.doi.org/10.1103/PhysRevB.54.11169>.
- [65] G. Kresse, J. Furthmuller, Efficiency of ab-initio total energy calculations for metals and semiconductors using a plane-wave basis set, *Comput. Mater. Sci.* 6 (1996) 15–50, [http://dx.doi.org/10.1016/0927-0256\(96\)00008-0](http://dx.doi.org/10.1016/0927-0256(96)00008-0).
- [66] G. Kresse, J. Hafner, Ab initio molecular-dynamics simulation of the liquid-metal–amorphous-semiconductor transition in germanium, *Phys. Rev. B* 49 (1994) 14251–14269, <http://dx.doi.org/10.1103/PhysRevB.49.14251>.
- [67] G. Kresse, J. Hafner, Ab initio molecular dynamics for liquid metals, *Phys. Rev. B* 47 (1993) 558–561, <http://dx.doi.org/10.1103/PhysRevB.47.558>.
- [68] P.E. Blöchl, Projector augmented-wave method, *Phys. Rev. B* 50 (1994) 17953–17979, <http://dx.doi.org/10.1103/PhysRevB.50.17953>.
- [69] G. Kresse, D. Joubert, From ultrasoft pseudopotentials to the projector augmented-wave method, *Phys. Rev. B* 59 (1999) 1758–1775, <http://dx.doi.org/10.1103/PhysRevB.59.1758>.
- [70] J.P. Perdew, K. Burke, M. Ernzerhof, Generalized gradient approximation made simple, *Phys. Rev. Lett.* 77 (1996) 3865–3868, <http://dx.doi.org/10.1103/PhysRevLett.77.3865>.
- [71] J.P. Perdew, K. Burke, M. Ernzerhof, Generalized gradient approximation made simple, *Phys. Rev. Lett.* 78 (1997) 1396, <http://dx.doi.org/10.1103/PhysRevLett.78.1396> vol.77, pg 3865, 1996.
- [72] G. Kresse, Recommended PAW Potentials for DFT Calculations Using vasp.5.2, (n.d.).
- [73] H.J. Monkhorst, J.D. Pack, Special points for brillouin-zone integrations, *Phys. Rev. B* 13 (1976) 5188–5192, <http://dx.doi.org/10.1103/PhysRevB.13.5188>.
- [74] J.D. Pack, H.J. Monkhorst, Special points for Brillouin-zone integrations - reply, *Phys. Rev. B* 16 (1977) 1748–1749, <http://dx.doi.org/10.1103/PhysRevB.16.1748>.
- [75] S.V. Khare, R.V. Kulkarni, D. Stroud, J.W. Wilkins, Energetics and bias-dependent scanning tunneling microscopy images of Si ad-dimers on Ge(001), *Phys. Rev. B* 60 (1999) 4458–4461, <http://dx.doi.org/10.1103/PhysRevB.60.4458>.
- [76] J.A. Warner, S.K.R. Patil, S. V. Khare, K.C. Masiulaniec, Ab initio calculations for properties of MAX phases Ti<sub>2</sub>TiC, Zr<sub>2</sub>TiC, and Hf<sub>2</sub>TiC, *Appl. Phys. Lett.* 88 (2006), <http://dx.doi.org/10.1063/1.2182009>.
- [77] I. Efthimiopoulos, J. Kemichick, X. Zhou, S.V. Khare, D. Ikuta, Y.J. Wang, High-pressure studies of Bi<sub>2</sub>S<sub>3</sub>, *J. Phys. Chem.* 118 (2014) 1713–1720, <http://dx.doi.org/10.1021/jp4124666>.
- [78] Z.T.Y. Liu, D. Gall, S.V. Khare, Electronic and bonding analysis of hardness in pyrite-type transition-metal pernitrides, *Phys. Rev. B* 90 (2014), <http://dx.doi.org/10.1103/PhysRevB.90.134102> 134102.
- [79] Z.T.Y. Liu, pyvasp-workflow, a simple yet flexible programmatic workflow of describing, submitting and analyzing VASP jobs, (n.d.). <https://github.com/terencezl/pyvasp-workflow> (accessed February 15, 2017).
- [80] Z.T.Y. Liu, pydass\_vasp, convenient Python modules and wrapping executable scripts, [https://github.com/terencezl/pydass\\_vasp](https://github.com/terencezl/pydass_vasp), (2015), Accessed date: 15 February 2017.
- [81] S.P. Ong, W.D. Richards, A. Jain, G. Hautier, M. Kocher, S. Cholia, D. Gunter, V.L. Chevrier, K.A. Persson, G. Ceder, Python Materials Genomics (pymatgen): a robust, open-source python library for materials analysis, *Comput. Mater. Sci.* 68 (2013) 314–319, <http://dx.doi.org/10.1016/j.commatsci.2012.10.028>.
- [82] F. Birch, Finite elastic strain of cubic crystals, *Phys. Rev.* 71 (1947) 809–824 <http://link.aps.org/doi/10.1103/PhysRev.71.809>.
- [83] F. Birch, Finite strain isotherm and velocities for single-crystal and polycrystalline NaCl at high-pressures and 300-degree-K, *J. Geophys. Res.* 83 (1978) 1257–1268, <http://dx.doi.org/10.1029/Jb083ib03p01257>.
- [84] M. Mehl, J. Osburn, D. Papaconstantopoulos, B. Klein, Erratum: structural properties of ordered high-melting-temperature intermetallic alloys from first-principles total-energy calculations, *Phys. Rev. B* 42 (1990) 5362–5363, <http://dx.doi.org/10.1103/PhysRevB.42.5362>.
- [85] Y. Tian, B. Xu, Z. Zhao, Microscopic theory of hardness and design of novel superhard crystals, *Int. J. Refract. Metals Hard Mater.* 33 (2012) 93–106, <http://dx.doi.org/10.1016/j.ijrmhm.2012.02.021>.
- [86] P. Deus, H.A. Schneider, Estimation of the debye temperature of diamond-like semiconducting compounds from bulk modul and microhardness, *Cryst. Res. Technol.* 18 (1983) 491–500, <http://dx.doi.org/10.1002/crat.2170180410>.
- [87] L.C. Zhou, F. Kormann, D. Holec, M. Bartosik, B. Grabowski, J. Neugebauer, P.H. Mayrhofer, Structural stability and thermodynamics of CrN magnetic phases from ab initio calculations and experiment, *Phys. Rev. B* 90 (2014), <http://dx.doi.org/10.1103/PhysRevB.90.184102>.
- [88] W. Arnaldsson Tang Chill, S. Henkelman, G.A. Bader. Charge Analysis, (n.d.). <http://theory.cm.utexas.edu/bader/>.
- [89] G. Henkelman, A. Arnaldsson, H. Jonsson, A fast and robust algorithm for Bader decomposition of charge density, *Comput. Mater. Sci.* 36 (2006) 354–360, <http://dx.doi.org/10.1016/j.commatsci.2005.04.010>.
- [90] E. Sanville, S.D. Kenny, R. Smith, G. Henkelman, Improved grid-based algorithm for Bader charge allocation, *J. Comput. Chem.* 28 (2007) 899–908, <http://dx.doi.org/10.1002/jcc.20575>.
- [91] W. Tang, E. Sanville, G. Henkelman, A grid-based Bader analysis algorithm without lattice bias, *J. Phys. Condens. Matter* 21 (2009) 84204, <http://dx.doi.org/10.1088/0953-8984/21/8/084204>.
- [92] R.F.W. Bader, *Atoms in Molecules: a Quantum Theory*, Oxford University Press, New York, 1990.
- [93] F.W. Bieglerkonig, R.F.W. Bader, T.H. Tang, Calculation of the average properties of atoms in molecules -2, *J. Comput. Chem.* 3 (1982) 317–328, <http://dx.doi.org/10.1002/Jcc.540030306>.
- [94] P.E. Blöchl, O. Jepsen, O.K. Andersen, Improved tetrahedron method for brillouin-zone integrations, *Phys. Rev. B* 49 (1994) 16223–16233, <http://dx.doi.org/10.1103/PhysRevB.49.16223>.
- [95] A. Togo, I. Tanaka, First principles phonon calculations in materials science, *Scripta Mater.* 108 (2015) 1–5, <http://dx.doi.org/10.1016/J.SCRIPAMAT.2015.07.021>.
- [96] H. Jacobs, D. Rechenbach, U. Zachwieja, Structure determination of Gamma-Fe<sub>4</sub>N and Epsilon-Fe<sub>3</sub>N, *J. Alloy. Comp.* 227 (1995) 10–17, [http://dx.doi.org/10.1016/0925-8388\(95\)01610-4](http://dx.doi.org/10.1016/0925-8388(95)01610-4).
- [97] C.A. Kuhnen, R.S. Defigueiredo, V. Drago, E.Z. Dasilva, Mossbauer studies and electronic-structure of Gamma-Fe<sub>4</sub>N, *J. Magn. Magn Mater.* 111 (1992) 95–104, [http://dx.doi.org/10.1016/0304-8853\(92\)91062-X](http://dx.doi.org/10.1016/0304-8853(92)91062-X).
- [98] J.F. Nye, *Physical Properties of Crystals: Their Representation by Tensors and Matrices*, Clarendon Press, 1985, <http://books.google.com/books?id=ugwql-uVB44C>.
- [99] F. Mouhat, F.-X. Coudert, Necessary and sufficient elastic stability conditions in various crystal systems, *Phys. Rev. B* 90 (2014) 224104, <http://dx.doi.org/10.1103/PhysRevB.90.224104>.
- [100] A.L. Ivanovskii, Mechanical and electronic properties of diborides of transition 3d-5d metals from first principles: toward search of novel ultra-incompressible and superhard materials, *Prog. Mater. Sci.* 57 (2012) 184–228, <http://dx.doi.org/10.1016/j.pmatsci.2011.05.004>.
- [101] M. Lopuszynski, J.A. Majewski, Ab initio calculations of third-order elastic constants and related properties for selected semiconductors, *Phys. Rev. B* 76 (2007), <http://dx.doi.org/10.1103/PhysRevB.76.045202>.
- [102] N.H. Miao, B.S. Sa, J.A. Zhou, Z.M. Sun, Theoretical investigation on the transition-metal borides with Ta<sub>3</sub>Ba-type structure: a class of hard and refractory materials, *Comput. Mater. Sci.* 50 (2011) 1559–1566, <http://dx.doi.org/10.1016/J.Commat.2010.12.015>.
- [103] S.F. Pugh, Relations between the elastic moduli and the plastic properties of polycrystalline pure metals, London, Edinburgh, Dublin Philos. Mag. J. Sci. 45 (1954) 823–843, <http://dx.doi.org/10.1080/14786440808520496>.
- [104] D.G. Pettifor, Theoretical predictions of structure and related properties of intermetallics, *Mater. Sci. Technol.* 8 (1992) 345–349.
- [105] D.G. Sangiovanni, L. Hultman, V. Chirita, Supertoughening in B1 transition metal nitride alloys by increased valence electron concentration, *Acta Mater.* 59 (2011) 2121–2134, <http://dx.doi.org/10.1016/J.Actamat.2010.12.013>.
- [106] D.G. Sangiovanni, V. Chirita, L. Hultman, Electronic mechanism for toughness enhancement in Ti<sub>3</sub>M<sub>(1-x)N</sub> (M = Mo and W), *Phys. Rev. B Condens. Matter* 81 (2010) 1–7, <http://dx.doi.org/10.1103/PhysRevB.81.104107>.
- [107] F.A. Lindemann, The calculation of molecular vibration frequencies, *Phys. Z.* 11 (1910) 609–612.
- [108] A. Zaoui, S. Kacimi, B. Bouhafs, A. Roula, First-principles study of bonding mechanisms in the series of Ti, V, Cr, Mo, and their carbides and nitrides, *Phys. B Condens. Matter* 358 (2005) 63–71, <http://dx.doi.org/10.1016/j.physb.2004.12.027>.
- [109] M.G. Brik, C.G. Ma, First-principles studies of the electronic and elastic properties of metal nitrides XN (X = Sc, Ti, V, Cr, Zr, Nb), *Comput. Mater. Sci.* 51 (2012) 380–388, <http://dx.doi.org/10.1016/j.commatsci.2011.08.008>.
- [110] Z.Y. Jiao, Y.J. Niu, S.H. Ma, X.F. Huang, Structural, elastic and mechanical properties of TMN (TM = Ti, V, Cr): a dft study, *Mod. Phys. Lett. B* 27 (2013), <http://dx.doi.org/10.1142/S0217984913501583>.
- [111] B. Alling, T. Marten, I.A. Abrikosov, Effect of magnetic disorder and strong electron correlations on the thermodynamics of CrN, *Phys. Rev. B* 82 (2010), <http://dx.doi.org/10.1103/PhysRevB.82.184430>.
- [112] B. Alling, T. Marten, I.A. Abrikosov, Questionable collapse of the bulk modulus in CrN, *Nat. Mater.* 9 (2010) 283–284, <http://dx.doi.org/10.1038/nmat2723>.
- [113] S.M. Wang, X.H. Yu, J.Z. Zhang, M. Chen, J.L. Zhu, L.P. Wang, D.W. He, Z.J. Lin, R.F. Zhang, K. Leinenweber, Y.S. Zhao, Experimental invalidation of phase-transition-induced elastic softening in CrN, *Phys. Rev. B* 86 (2012), <http://dx.doi.org/10.1103/PhysRevB.86.064111>.
- [114] A.L. Allred, E.G. Rochow, A scale of electronegativity based on electrostatic force, *J. Lncrg. Nucl. Chem.* 5 (1958) 264–268, [http://dx.doi.org/10.1016/0022-1902\(58\)80003-2](http://dx.doi.org/10.1016/0022-1902(58)80003-2).
- [115] Tandy Supercomputing Center (TSC), (n.d.). <https://portal.oii.org/display/desktop/Acknowledgement+Policy> (accessed June 7, 2017).
- [116] Ohio Supercomputer Center, (n.d.). <http://osc.edu/ark:/19495/fs1ph73> (accessed June 7, 2017).